International Journal of Thermophysics, Vol. 21, No. 1, 2000

Semiempirical Estimation of Thermal Expansion Coefficients and Isobaric Heat Capacities of Fluorite-Type Compounds

H. Inaba[1]

Received April 29, 1999

The thermal expansion coefficients and isobaric heat capacities of fluorite-type compounds have been estimated using the Morse potential and the Debye model. The Born repulsion parameters of various compounds, which are necessary for determining the parameters of the Morse potential, have been determined empirically for elements belonging to every period of the periodic table. Using the parameters thus determined, the Debye temperature, the thermal expansion coefficient, and the Gruneisen constant of fluorite-type compounds have been calculated and then the isochoric and the isobaric heat capacities have been calculated over a wide range of temperatures. The calculated thermal expansion coefficients and isobaric heat capacities thus obtained are in good agreement with experimental values except for the anomalous temperature regions due to vacancy formation and phase transitions.

KEY WORDS: Debye model; Debye temperature; fluorite; Gruneisen constant; heat capacity; Morse potential; oxides; thermal expansion; vacancy formation.

1. INTRODUCTION

The properties required of materials have become increasingly sophisticated, and combinations of various materials such as composites of metals and ceramics, metal–ceramic bonding, and various coatings have been developed to meet such demands. When such combinations of materials are used at high temperatures, it is necessary for them to have almost the same thermal expansion coefficients over the temperature range used. Thus,

[1] Department of Science Education, Faculty of Education, Chiba University, 1-33 Yayoi-Chou, Inage-Ku, Chiba 263-8522, Japan.

0195-928X/00/0100-0249$18.00/0 © 2000 Plenum Publishing Corporation

estimation of the thermal expansion coefficients of materials has become increasingly important to design a system composed of composite materials. Not only for such a practical purpose but also from a theoretical point of view, the estimation of the thermal expansion coefficient of materials is important, because the thermal expansion coefficient is one of the most important thermodynamic quantities. Theoretical calculations of the thermal expansion coefficients of inorganic materials have been made [1–5] by the use of potential models. These calculations, however, usually require many fitting parameters or the coefficients of the potential to be determined and are usually difficult to apply to other types of compounds.

Ruffa [6, 7] proposed a rather general method for the calculation of thermal expansion coefficients, which can easily be applied to various inorganic materials. He utilized the Morse potential and the Debye model for the frequency distribution of the Morse oscillator. His method successfully explained the temperature dependence of the thermal expansion coefficient, but some of the calculated values did not agree with measurements due to inappropriate values of parameters used in the calculation.

Calculation of phase diagrams (CALPHAD method) has become increasingly important not only from a practical viewpoint but also for assessment of experimental thermodynamic data. Although the CALPHAD method is a powerful technique to interpret thermodynamic phenomena, the assessed thermodynamic data are still limited for users. For assessment of experimental thermodynamic data, heat capacity data at high temperatures are very important. However, accurate measurement of the heat capacity at high temperatures is very difficult because of a rapid increase in radiative heat transfer. Theoretical estimation of the isochoric heat capacity is possible by using the Debye model. This model, however, is not so effective at high temperatures, since the heat capacity increases only slightly above room temperature according to the model, while the experimental heat capacity increases significantly above room temperature. Since the measured heat capacity is an isobaric heat capacity, the dilational contribution to the heat capacity becomes important above room temperature. It is thermodynamically expressed as [8]

$$C_d = C_p - C_v = (V\beta^2/B_T)\, T = \gamma\beta C_v T \tag{1}$$

where C_p and C_v are the isobaric and isochoric heat capacities, V is the molar volume, β is the volume thermal expansion coefficient, B_T is the isothermal bulk modulus, and γ is the Gruneisen constant. The dilational heat capacity has usually been estimated using an empirical equation such as the Nernst–Lindemann equation. It would be more desirable, however, if the dilational contribution can be properly estimated using Eq. (1).

The estimation of the dilational heat capacity is also important to analyze an observed heat capacity at high temperatures. In order to separate the excess heat capacity such as due to vacancy formation, and dielectric and magnetic contributions, estimation of the dilational contributions, as well as the vibrational contribution, is necessary.

The present author [9–11] has reported a method to estimate the thermal expansion coefficient of inorganic compounds by using the Morse potential and the Debye model. The method was originally developed by Ruffa [6, 7] and was improved by the author by reevaluating the parameters used. The method has also been extended to estimate the dilational and the isobaric heat capacity using Eq. (1) [12].

In this paper, the method to estimate the thermal expansion coefficient and the isobaric heat capacity is presented using the Morse potential and the Debye model and is applied to fluorite-type compounds.

2. THEORY

In order to estimate the thermal expansion coefficient and the isobaric heat capacity, we utilize the Morse potential [6, 7]. The Morse potential $V(r)$ can be expressed as

$$V(r) = D[\exp\{-2a(r-r_0)\} - 2\exp\{-a(r-r_0)\}] \tag{2}$$

where D is the depth of the potential, r is the interatomic separation, r_0 is the interatomic separation at the potential minimum, and a is the inverse line width of the potential. The first term in the square bracket represents repulsion and the second term represents attraction. The frequency v for the Morse oscillator can be expressed as

$$v = (a/\pi)(D/2\mu)^{1/2} \tag{3}$$

where μ is the reduced mass of the oscillator. The vibrational energy E_n and the mean atomic separation $\langle r_n \rangle$ of the motion with the principal quantum number n of this oscillator can be expressed as

$$E_n = hv(n+1/2) - \{(hv)^2/4D\}(n+1/2)^2 \tag{4}$$

$$\langle r_n \rangle = r_0 + (hv/2aD)(n+3/4) + \mathrm{O}(v^2) \tag{5}$$

where h is the Planck constant and $\mathrm{O}(v^2)$ is the quadratic vibrational term. The statistical mean interatomic separation of the oscillator at temperature T can be given, temporarily neglecting the quadratic vibrational term in Eq. (5), as

$$\bar{r} = \sum_{m=0}^{\infty} \langle r_m \rangle \exp(-E_m/kT) \Big/ \sum_{m=0}^{\infty} \exp(-E_m/kT) \tag{6}$$

$$= r_0 + (3hv/8aD) + (hv/2aD)\{\exp(hv/kT) - 1\}^{-1} \tag{7}$$

where k is the Boltzmann constant. The second term in Eq. (7) represents the deviation from the equilibrium position due to the zero-point vibration and the third term is associated with thermal vibration. If we assume that the vibrational frequency distribution of a crystal is described by the Debye model, we can evaluate the thermal expansion of the crystal by averaging the third term in Eq. (7) with respect to the vibrational frequency from $v = 0$ to $v = v_D$ (Debye frequency).

The mean interatomic separation at temperature T for the Morse oscillator can be given, assuming the Debye model for the frequency distribution of the oscillator, as

$$\langle \bar{r} \rangle = \frac{1}{3N} \int_0^{v_D} f(v)\, dv \frac{hv}{2aD} \{\exp(hv/kT) - 1\}^{-1}$$

$$= (3kT/2aD)(T/\theta_D)^3 f_1(x_D) \tag{8}$$

$$f_1(x_D) = \int_0^{x_D} \frac{x^3\, dx}{\exp(x) - 1}, \qquad x = hv/kT, \qquad x_D = hv_D/kT = \theta_D/T \tag{9}$$

where θ_D is the Debye temperature. $f(v)\, dv$ is the number of vibration modes, and it is proportional to $v^2\, dv$ according to the Debye model. Thus, the linear thermal expansion coefficient of the crystal composed of $3N$ Morse oscillators can be expressed as

$$\alpha_1(T) = \frac{d}{dT}\left(\frac{\langle \bar{r} \rangle}{r_n}\right) = \frac{3k}{2ar_nD}\left(\frac{T}{\theta_D}\right)^3 g_1(x_D) \tag{10}$$

$$g_1(x_D) = \int_0^{x_D} \frac{x^4 e^x}{(e^x - 1)^2}\, dx \tag{11}$$

where r_n is the equilibrium interatomic separation of the oscillator and Eq. (11) is known as the Debye function.

Equation (10) can be compared with the equation for the volume thermal expansion coefficient β derived from the known thermodynamic relation [8]:

$$\beta = \frac{\gamma C_v}{V B_T} \tag{12}$$

where V, B_T, and γ are the same symbols as those in Eq. (1). The thermal expansion coefficient has the term C_V and its temperature dependence is almost the same as C_V, since the proportional coefficient is independent of temperature in Eq. (10) and it varies only slightly with temperature in Eq. (12).

Taking into account the higher term of the thermal oscillation in Eq. (10) as

$$\alpha_2(T) = \frac{2k^2T}{4ar_nD^2}\left(\frac{T}{\theta_D}\right)^3 g_2(x_D) \tag{13}$$

$$g_2(x_D) = \int_0^{x_D} \frac{x^5e^x(1+e^x)}{(e^x-1)^3}\,dx \tag{14}$$

Then the linear thermal expansion coefficient including the correction term can be expressed as

$$\alpha(T) = \alpha_1(T) + \alpha_2(T) \tag{15}$$

In order to apply these equations to various compounds we need to know the parameters of the Morse potential: D, a, r_0, and the Debye temperature, θ_D. For this purpose, Ruffa [6, 7] used the Born potential, which has generally been used for ionic crystals as

$$V_B(r) = -A/r + B/r^m \tag{16}$$

$$A = Ne^2z^2\alpha \tag{17}$$

where m, α, e, z, and N are the coefficient of Born repulsion, the Madelung constant, the electric charge, the ion valence, and Avogadro's number, respectively. It can be written for the equilibrium distance r_n as

$$V_B(r_n) = -A/r_n[1-(1/m)] \tag{18}$$

In order to relate the Born potential and the Morse potential, Ruffa [6, 7] used the following empirical equations:

$$D = 0.1\,V_B(r_n) \tag{19}$$

$$ar_n = (m+4)/5 \tag{20}$$

the debye temperature, θ_D, can be obtained, using the following relation:

$$\theta_D = (h/k)\,v_D = (2ha/\pi k)(D/2\mu)^{1/2} \tag{21}$$

where μ is the reduced mass of the oscillator.

Table I. The m Parameters for Halides m_h and Oxides m_o for each Row in the Periodic Table Depending on the Existence of d- or f-Electrons for the Metal Elements of the Oxides

Row in the periodic table	m_h	m_o (typical)	m_o (transition)
II	6.05	7.27	—
III	8.59	8.07	—
IV	11.36	9.67	8.41
V	12.21	9.60	8.96
VI	13.38	9.88	9.18
VII	—	10.12	9.35

Ruffa [6, 7] determined the Born constant, m, for alkali halides using the compressibility data. However, as described in previous papers [9–11], some of the thermal expansion coefficients calculated using the values of m determined by Ruffa are very different from experimental values. For this reason, the parameter m for alkali halides was reevaluated in the previous study [9] by fitting the thermal expansion coefficients of alkali halides at 293 K to the experimental values. The thermal expansion coefficients of alkaline-earth fluorides obtained from the calculation using the m parameter thus determined are in good agreement with the experimental ones. It is not appropriate, however, to use the same m parameter for oxides, because the bonding character of oxides is quite different from that of halides and the m parameter should be different. The bonding character of oxides would be different from oxide to oxide but can be classified in several groups depending on the period of the periodic table and the existence of d- or f-electrons for the metal elements of oxides. The m parameter for oxides including actinide oxides was empirically determined so as to reproduce experimental thermal expansion coefficients at 293 K of some oxides as given in Table I [10, 11].

In order to estimate the dilational heat capacity, we need to estimate the Gruneisen parameter γ, which can be written as follows according to Ruffa [13]:

$$\begin{aligned}\gamma &= 5(5ar_n - 4)/(9ar_n)[1 + (kT/2D)\, F(T)] \\ &= 25m/\{9(m+4)\}[1 + (kT/2D)\, F(T)] \\ &= 25m/\{9(m+4)\}[1 + (kT/2D) \\ &\quad \times \{f_1(x_D) - (15/2)\, x_D^{-3} f(x_D)(m+3)/(m+4)\}] \end{aligned} \tag{22}$$

where $f(x_D)$, $f_1(x_D)$, x_D, and $F(T)$ are expressed as

$$f(x_D) = \int_0^{x_D} \frac{x^3}{(e^x - 1)}\, dx, \qquad f_1(x_D) = \int_0^{x_D} \frac{x^4(1 + e^x)}{(e^x - 1)^2}, \qquad x_D = \theta_D / T$$

$$F(T) = f_1(x_D)/f(x_D) - (15/2)\, x_D^{-3} f(x_D)(m + 3)/(m + 4)$$

Since the isochoric heat capacity can usually be regarded as the vibrational term, we use the Debye equation:

$$C_V = 9R(T/\theta_D)^3\, g_1(x_D) \tag{23}$$

where R is the gas constant.

Using Eqs. (1), (15), (22), and (23), we can estimate the dilational heat capacity and the isobaric heat capacity.

3. RESULTS AND DISCUSSION

The experimental [14] thermal expansion coefficient of CaF_2 and that calculated using Eq. (15) are shown in Fig. 1. It is shown that the experimental thermal expansion coefficient of CaF_2 is in excellent agreement with the calculated value at low temperatures but becomes larger at high temperatures. The excess part of the thermal expansion coefficient at high temperatures as considered to be due to the vacancy formation as described previously [9].

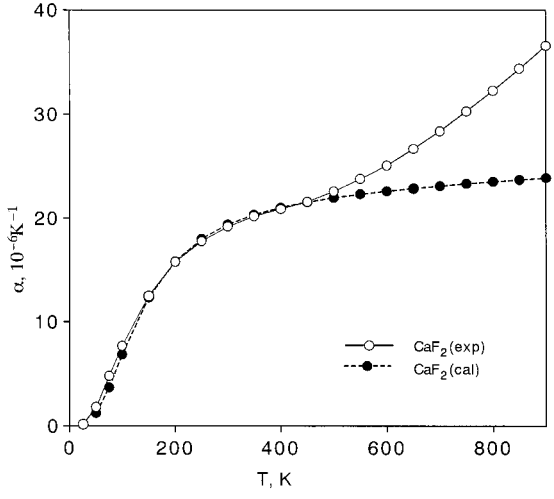

Fig. 1. Calculated and experimental [14] thermal expansion coefficients of CaF_2.

The experimental [14] thermal expansion coefficient of BaF_2 and that calculated using Eq. (15) are shown in Fig. 2. The experimental thermal expansion coefficient of BaF_2 is in agreement with the calculated value below 200 K but becomes larger above 400 K. the larger value of the thermal expansion coefficient above 400 K is considered to be due to the vacancy formation, similarly as in CaF_2.

The experimental [14, 15] thermal expansion coefficient of CeO_2 and that calculated using Eq. (15) are shown in Fig. 3. The two experimental thermal expansion coefficients are different at low temperatures. One reason for this may be due to the choice of a function to fit the thermal expansion data, since it is necessary to differentiate the regression function in order to obtain the thermal expansion coefficient. The calculated thermal expansion coefficient at low temperatures is smaller than the experimental value by Taylor [15]. There exist two possibilities for this difference. One is the larger estimation of the Debye temperature in the theoretical calculation, which comes from the larger value for the parameter m in Table I. The other is the error due to the use of the improper regression function at low temperatures to obtain the experimental thermal expansion coefficient. The larger thermal expansion coefficient at high temperatures for the experimental results is considered to be due to vacancy formation, similarly as in CaF_2.

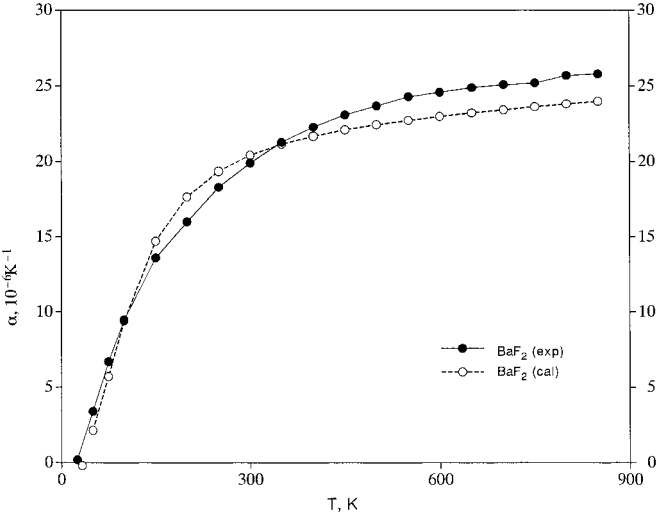

Fig. 2. Calculated and experimental [14] thermal expansion coefficients of BaF_2.

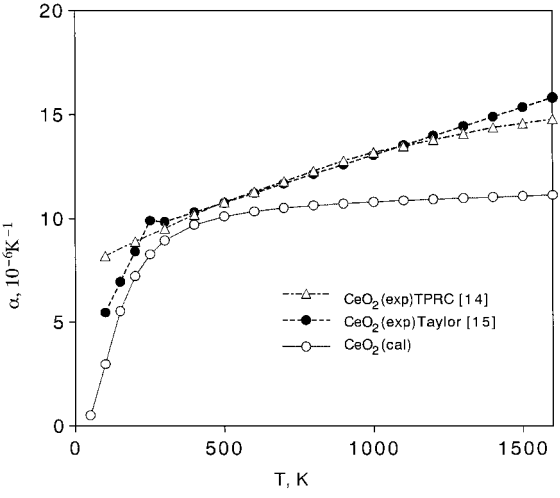

Fig. 3. Calculated and experimental thermal expansion coefficients of CeO_2.

The experimental [14–16] thermal expansion coefficient of ThO_2 and that calculated using Eq. (15) are shown in Fig. 4. The calculated thermal expansion coefficient at low temperatures is in relatively good agreement with the experimental value of Taylor [15]. The experimental thermal expansion coefficient at low temperatures by TPRC [14] is considerably larger than those of Taylor [15] and the calculated value. Since the temperature dependence of the thermal expansion coefficient at low temperatures should roughly obey the Debye function expressed by Eqs. (5) and (7), the results of Taylor [15] are considered to be relatively more reliable at low temperatures. The experimental data are in good agreement with the calculated values between 500 and 1000 K but are larger above 1000 K. The larger value of the thermal expansion coefficient at high temperatures is considered to be due to vacancy formation, similarly as in CaF_2.

The experimental [14–16] thermal expansion coefficient of UO_2 are shown in Fig. 5. The calculated thermal expansion coefficient at low temperatures is smaller then the experimental value measured by Taylor [15]. One reason for this may be due to the fact that the regression data for the thermal expansion used by Taylor were expressed by a quadratic function, which is inappropriate at low temperatures. The experimental data [14, 15] are in good agreement with the calculated values between 300 and 1000 K except for that of Momin and Karkhanavala [16]. The experimental data above 1000 K become considerably larger than the calculated values. The larger values of the thermal expansion coefficient at high temperatures,

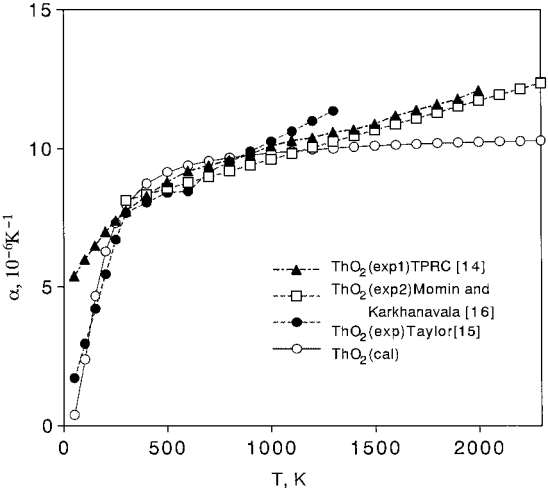

Fig. 4. Calculated and experimental thermal expansion coefficients of ThO_2.

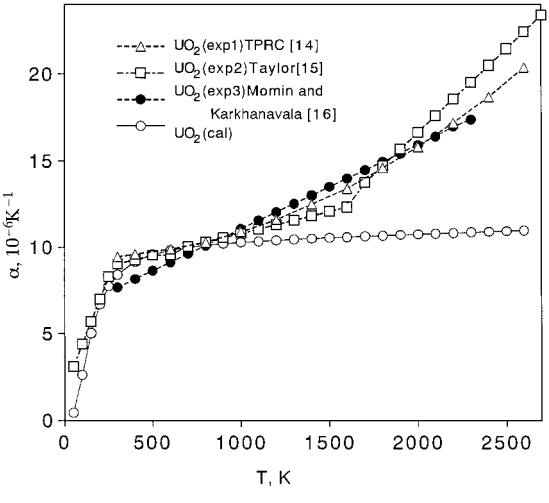

Fig. 5. Calculated and experimental thermal expansion coefficients of UO_2.

which are also seen in the heat capacity curve, have been attributed mainly to Frenkel defects in the oxygen sublattice.

The experimental [14, 15, 17, 18] thermal expansion coefficient of PuO_2 and that calculated using Eq. (15) are shown in Fig. 6. The calculated thermal expansion coefficient at low temperatures is slightly different from the experimental value measured by Taylor [15]. The reason for this may be the same as that given for UO_2. The calculated data are in good agreement with the experimental results [14, 15, 17, 18] between 300 and 1000 K. The experimental data become considerably larger than the calculated values above 1000 K for reasons similar to UO_2.

The Gruneisen constants of CaF_2, ThO_2, and UO_2 are calculated using Eq. (22) and the results are shown versus temperature in Figs. 7, 8, and 9, respectively. The calculated Gruneisen constant of CaF_2 is in good agreement with the experimental results of Bayley and Yates [19] and of Batchelder and Simmons [20] above 100 K, although they are slightly larger than those of White [21]. The calculated Gruneisen constant of ThO_2 is in excellent agreement with the experimental results [16] except for low temperatures. These results indicate that the calculation procedure using Eq. (22) is reasonable. The calculated Gruneisen constant of UO_2 is between 1.4 and 1.45 depending slightly on temperature, but the experimental values obtained by Momin and Karkhanavala [16] show a larger dependence on temperature ranging between 1.7 and 2.0, as shown in Fig. 9. The theoretical Gruneisen constant of UO_2 was also obtained as 1.86

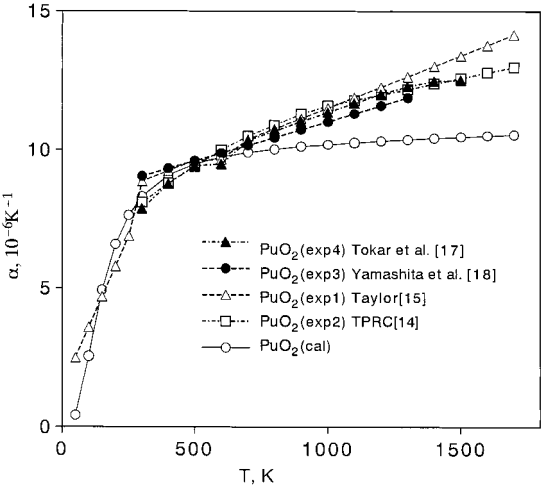

Fig. 6. Calculated and experimental thermal expansion coefficients of PuO_2.

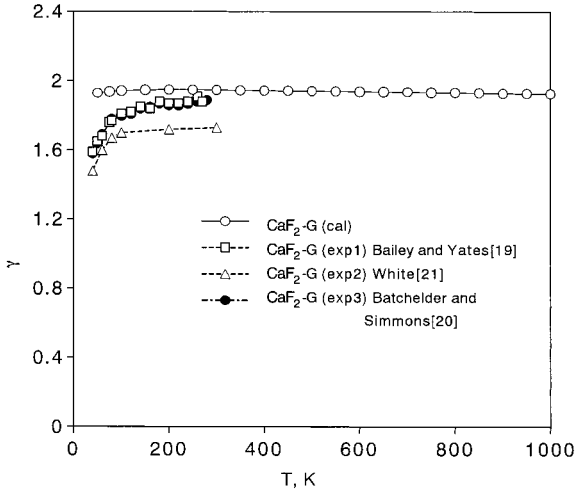

Fig. 7. Calculated and experimental Gruneisen constants of CaF_2.

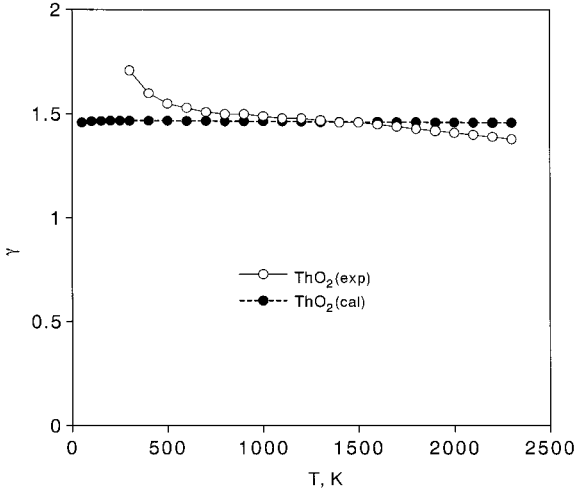

Fig. 8. Calculated and experimental [16] Gruneisen constants of UO_2.

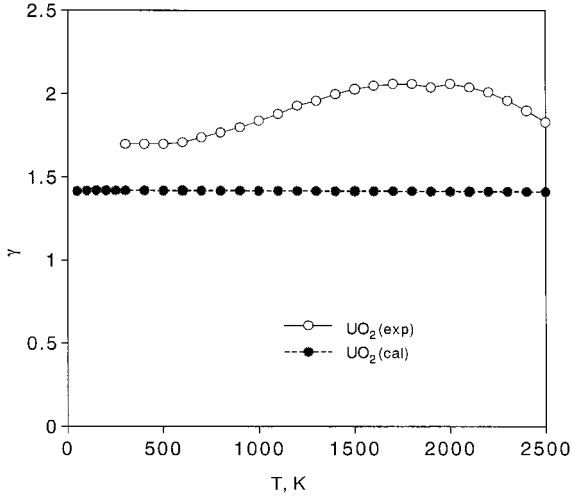

Fig. 9. Calculated and experimental [16] Gruneisen constants of UO_2.

and 1.28 by Singh and Pandy [22] and Singh et al. [23], respectively. The reason for these differences may lie in the uncertainty of both the theoretical and the experimental values. The main possible source of error in the calculations is the uncertainty of the parameters used in the calculations. The main possible source of error in the experiments is the uncertainty of the values of experimental quantities, such as Young's modulus, the Poisson ratio, the thermal expansion, and the heat capacity used to obtain the Gruneisen constant.

The isochoric and isobaric heat capacities of CaF_2 are calculated using Eqs. (1) and (21)–(23) and are shown in Fig. 10, where the experimental heat capacities [24, 25] are also shown for comparison. It is shown that the experimental heat capacity of CaF_2 [24] is slightly larger than the calculated value at low temperatures. This may be due to the larger estimation of the Debye temperature in the calculation. The experimental heat capacities are different at 300 K. The experimental heat capacity at 300 K measured by Todd [24], which is close to the calculated value, is considered to be more reliable than that by Naylor [25], since the data of Todd [24] were obtained by a direct heat capacity measurement. The experimental heat capacity becomes larger than the calculated value at high temperatures. The excess part at high temperatures is also seen in the thermal expansion coefficient in Fig. 1, and this is attributed to vacancy formation.

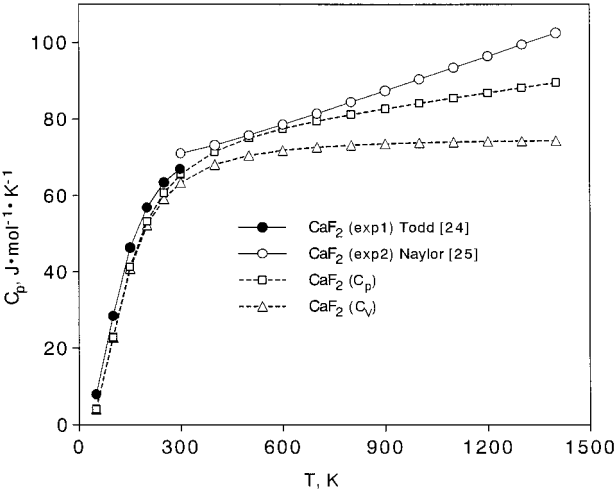

Fig. 10. Calculated isochoric (C_v) and isobaric (C_p) heat capacities and experimental heat capacities of CaF_2.

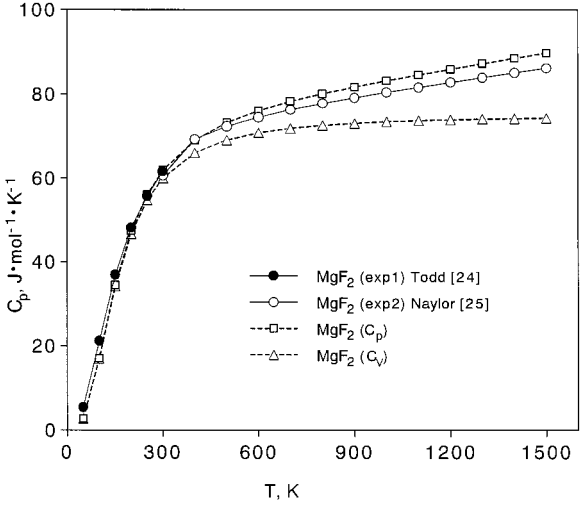

Fig. 11. Calculated isochoric (C_v) and isobaric (C_p) heat capacities and experimental heat capacities of MgF_2.

The isochoric and isobaric heat capacities of MgF_2 are calculated using Eqs. (1) and (21)–(23) and are shown in Fig. 11, where the experimental heat capacities [24, 25] are also shown for comparison. It is shown that the experimental heat capacity of MgF_2 [24] is slightly larger than the calculated value at low temperatures. The calculated isobaric heat capacity becomes close to the experimental value at high temperatures.

The isochoric and isobaric heat capacities of ZrO_2 are calculated using Eqs. (1) and (21)–(23) and are shown in Fig. 12, where the experimental heat capacities [26, 27] are also shown for comparison. It is shown that the experimental heat capacity of ZrO_2 [26] is slightly larger than the calculated value at low temperatures. The calculated isobaric heat capacity becomes close to the experimental value at high temperatures.

The isochoric and isobaric heat capacities of CeO_2 are calculated using Eqs. (1) and (21)–(23) and are shown in Fig. 13, where the experimental heat capacities [28, 29] are also shown for comparison. It is shown that the experimental heat capacity of CeO_2 [28] is slightly larger than the calculated value at low temperatures. The experimental heat capacity is close to the calculated value around 300 K and becomes larger at high temperatures. The excess part at high temperatures is considered to be due to vacancy formation.

The isochoric and isobaric heat capacities of ThO_2, UO_2, and PuO_2 are calculated using Eqs. (1) and (21)–(23) and are shown in Figs. 14, 15, and 16, respectively. The experimental heat capacities of ThO_2 [30], UO_2

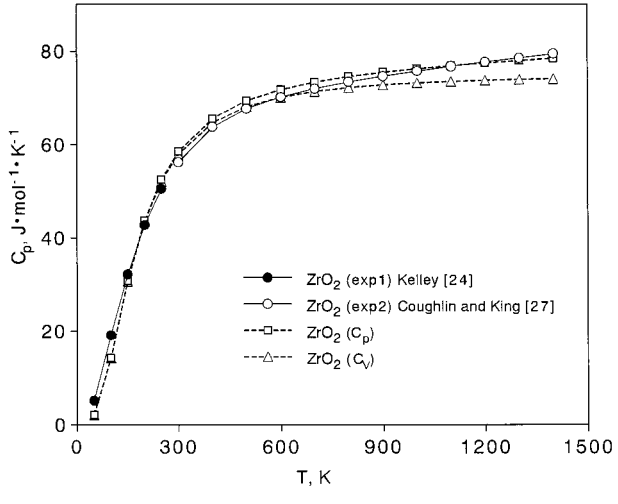

Fig. 12. Calculated isochoric (C_v) and isobaric (C_p) heat capacities and experimental heat capacities of ZrO_2.

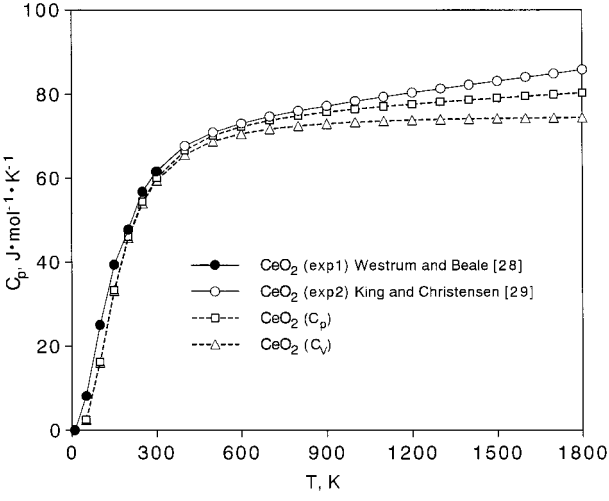

Fig. 13. Calculated isochoric (C_v) and isobaric (C_p) heat capacities and experimental heat capacities of CeO_2.

[31], and PuO_2 [32] at low temperatures were obtained from direct measurements. It is not possible, however, to obtain heat capacity data of these compounds at high temperatures by direct measurements, since only enthalpy data using drop calorimetry are available at high temperatures. We have to differentiate the smoothed enthalpy data by using a proper analytical or numerical function in order to obtain heat capacity values. Therefore, the heat capacity results are dependent on the choice of the function. The choice of the function is a matter of discussion [33–35], especially for the case of UO_2, in which the so-called Bredig transition exists at about 2610 K. In order to avoid this kind of complexity, we have restricted the temperature range to below 2600 K and have used the function proposed by Fink [35]. The reason for the use of this function is that the calculated value for UO_2 using his function is on good agreement with the direct heat capacity measurement by Gronvold et al. [36] at 1000 K. The function of the heat capacity for ThO_2, UO_2, and PuO_2 is shown in Ref. 35 as

$$C_p = C_1\theta^2 \exp(\theta/T)/\{T(\exp(\theta/T)-1\}^2 + 2C_2T + C_3k(1+E_a/kT)\exp(-E_a/kT) \quad (24)$$

where θ is the Einstein temperature, E_a is the activation energy, and C_1, C_2, and C_3 are constants. Using the values given by Fink [35] for these

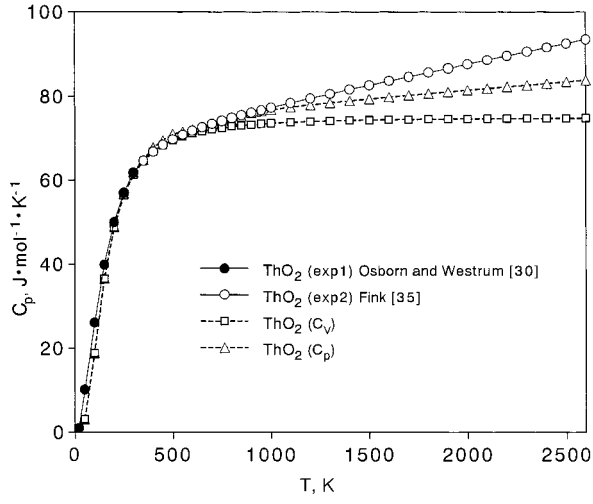

Fig. 14. Calculated isochoric (C_v) and isobaric (C_p) heat capacities and experimental heat capacities of ThO_2.

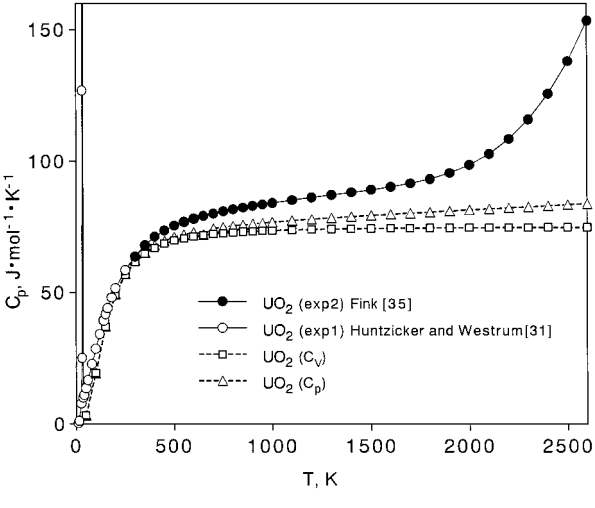

Fig. 15. Calculated isochoric (C_v) and isobaric (C_p) heat capacities and experimental heat capacities of UO_2.

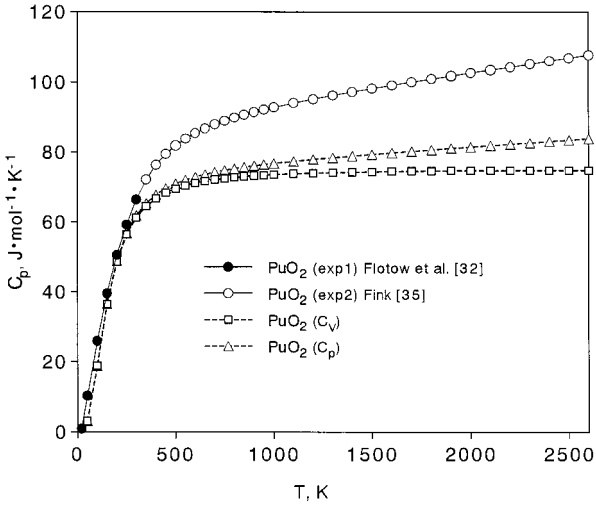

Fig. 16. Calculated isochoric (C_v) and isobaric (C_p) heat capacities and experimental heat capacities of PuO_2.

constants, the heat capacities of ThO_2, UO_2, and PuO_2 were calculated between 300 and 2600 K and are plotted as the experimental values in Figs. 14, 15, and 16, respectively.

As shown in Fig. 14, the experimental isobaric heat capacity of ThO_2 is slightly larger than the calculated value below 200 K, approaching the calculated value between 200 and 1200 K and then becoming larger at higher temperatures. The smaller calculated heat capacity at low temperatures may be due to the larger estimation of the Debye temperature in the calculation. The larger experimental heat capacity above 1200 K may be attributed to the excess heat capacity from the formation of Frenkel oxygen defects, which was suggested by the neutron diffuse and inelastic scattering experiments by Hatchings [37].

As shown in Fig. 15, the experimental heat capacity of UO_2 [31] shown a sharp transition at 30.44 K, which was considered to be of an antiferromagnetic origin. It is also shown in Fig. 15 that the experimental isobaric heat capacity is larger than the calculated value at low temperatures, approaching the calculated value around 300 K and then becoming increasingly larger at higher temperatures. The smaller calculated heat capacity at low temperatures may be due to the larger estimation of the Debye temperature in the calculation. The larger experimental heat capacity compared with the calculated value at high temperatures is due to an excess heat capacity, the origin of which has been a matter of discussion.

The excess heat capacity has been attributed to the electronic excitation and/or the formation of Frenkel oxygen defects. As was discussed using the data by neutron diffuse and inelastic scattering experiments [37], the main contribution of the excess heat capacity is possibly due to the formation of Frenkel oxygen defects, especially at high temperatures, above 200 K. There still exists a small excess heat capacity at lower temperatures, around 500 K and above, which may be due to the electronic excitation as discussed by Gronvold et al. [36] and Osborne et al. [38]. Therefore, it is concluded that the excess heat capacity may be the effect of a small contribution of the electronic excitation and an increasingly larger contribution of the formation of Frenkel oxygen defects as the temperature increases.

As shown in Fig. 16, the experimental isobaric heat capacity of PuO_2 is slightly larger than the calculated value at low temperatures and then becomes larger at higher temperatures. The excess heat capacity of PuO_2 at higher temperatures is not as large as that of UO_2. The origin of the excess heat capacity of PuO_2 may also be due to the electronic excitation and the formation of Frenkel oxygen defects, although these contributions are not known quantitatively.

4. CONCLUSIONS

The thermal expansion coefficients, Gruneisen constants, and isobaric heat capacities of fluorite-type compounds have been calculated semi empirically using the Morse potential and the Debye model.

1. The calculated thermal expansion coefficients of CaF_2, BaF_2, ThO_2, UO_2, and PuO_2 are in good agrement with the experimental results except for the excess part of the experimental results due to vacancy formation at high temperatures.
2. The calculated Gruneisen constants of CaF_2 and ThO_2 are in good agrement with the experimental results, although that of UO_2 is different from the experimental value, probably due to both the uncertainty in the parameters used in the calculation and the thermophysical property values used to derive the experimental result.
3. The calculated isobaric heat capacities of CaF_2, MgF_2, ZrO_2, CeO_2, ThO_2, UO_2, and PuO_2 are in good agreement with the experimental results, except for the anomalous heat capacities due to vacancy formation and phase transitions.

REFERENCES

1. R. R. Reeber, *Phys. Stat. Solids a* **32**:321 (1975).
2. K. Wang and R. R. Reeber, *J. Phys. Chem. Solids* **56**:895 (1995).
3. Z. Gong, G. K. Horton, and E. R. Cowley, *Phys. Rev.* **40**:3294 (1989).
4. L. L. Boyer, *Phys. Rev. Lett.* **42**:584 (1979).
5. M. P. Madan, *Physica* **12B**:35 (1984).
6. A. R. Ruffa, *J. Mater. Sci.* **15**:2258 (1980).
7. A. R. Ruffa, *J. Mater. Sci.* **15**:2268 (1980).
8. Y. S. Touloukian and E. H. Buyco, *Thermophysical Properties of Matter*, *Vol. 5. Specific Heat of Nonmetallic Solids* (Plenum, New York, 1970).
9. H. Inaba, *J. J. Appl. Phys.* **35**:3522 (1996).
10. H. Inaba, *J. J. Appl. Phys.* **35**:4730 (1996).
11. H. Inaba and H. Tagawa, *J. Ceram. Soc. Japan* **35**:4730 (1996).
12. H. Inaba, *J. Phase Equil.* **20**:187 (1999).
13. A. R. Ruffa, *J. Chem. Phys.* **83**:6405 (1985).
14. Y. S. Touloukian, R. K. Kibby, R. E. Taylor, and T. Y. R. Lee, *Thermophysical Properties of Matter*, *Vol. 13. Thermal Expansion of Nonmetallic Solids* (Plenum, New York, 1970).
15. D. Taylor, *Br. Ceram. Trans. J.* **83**:32 (1984).
16. A. C. Momin and M. D. Karkhanavala, *High Temp. Sci.* **10**:45 (1978).
17. M. Tokar, A. W. Nutt, and T. K. Keenan, *Nucl. Technol.* **17**:147 (1973).
18. T. Yamashita, H. Muto, T. Tsuji, and Y. Nakamura, *J. Alloys Comp.* **271**–**273**:404 (1988).
19. A. C. Bailey and B. Yates, *Proc. Phys. Soc.* **91**:390 (1967).
20. D. N. Batchelder and R. O. Simmons, *J. Chem Phys.* **41**:2327 (1964).
21. G. K. White, *J. Phys. C Solid State Phys.* **13**:4905 (1980).
22. R. K. Singh and N. K. Pandy, *Phys. Stat. Solids b* **115**:555 (1983).
23. R. K. Singh, S. P. Sanyal, and N. K. Pandy, *J. Chem Phys.* **67**:2596 (1982).
24. S. S. Todd, *J. Am. Chem. Soc.* **71**:4115 (1949).
25. B. F. Naylor, *J. Am. Chem. Soc.* **67**:150 (1945).
26. K. K. Kelley, *Ind. Eng. Chem.* **36**:377 (1944).
27. J. P. Coughlin and E. G. King, *J. Am. Chem. Soc.* **72**:2262 (1950).
28. E. F. Westrum and A. F. Beale, *J. Phys. Chem.* **65**:353 (1961).
29. E. G. King and A. U. Christensen, *U.S. Bur. Mines Rep. Invest.* **RI-5789**:1 (1961).
30. D. W. Osborne and E. F. Westrum, *J. Chem. Phys.* **21**:1884 (1953).
31. J. J. Huntzicker and E. F. Westrum, *J. Chem. Thermodyn.* **3**:61 (1971).
32. H. L. Flotow, D. W. Osborne, S. M. Fried, and J. G. Malm, *J. Chem. Phys.* **65**:1124 (1976).
33. G. L. Hyland and R. W. Ohse, *J. Nucl. Mater.* **140**:149 (1986).
34. J. Ralph, *J. Chem. Soc. Faraday Trans.* 2 **83**:1253 (1987).
35. J. K. Fink, *Int. J. Thermophys.* **3**:165 (1982).
36. F. Gronvold, N. J. Kveseth, A. Sveen, and J. Tichy, *J. Chem. Thermodyn.* **2**:665 (1970).
37. M. T. Hatchings, *J. Chem. Soc. Faraday Trans.* 2 **83**:1083 (1987).
38. R. Osborne, B. C. Boland, Z. A. Bowden, A. D. Tayler, M. A. Hackett, W. Hayes, and M. T. Hatchings, *J. Chem. Soc. Faraday Trans.* 2 **83**:1105 (1987).